Available online at www.sciencedirect.com
ScienceDirect
Journal of Solid State Chemistry 179 (2006) 3136–3144
JOURNAL OF SOLID STATE CHEMISTRY
www.elsevier.com/locate/jssc

Four triazole-bridging coordination polymers containing (*m*-phenol)-1,2,4-triazole: Syntheses, structures and properties of fluorescence and magnetism

Bing Liu, Guo-Cong Guo*, Jin-Shun Huang

State Key Laboratory of Structural Chemistry, Fujian Institute of Research on the Structure of Matter, Chinese Academy of Sciences, Fuzhou, Fujian 350002, People's Republic of China

Received 18 March 2006; received in revised form 12 May 2006; accepted 28 May 2006
Available online 14 June 2006

Abstract

Four triazole-bridging coordination complexes, $[Zn_4(ptr)_2(SO_4)_3(\mu_3\text{-}OH)_2(H_2O)_4]_n$ (**1**), $[Hg(CN)_2(ptr)]_n$ (**2**), $[Hg(Cl)_2(ptr)]_n$ (**3**), and $[Cu_2(\mu_2\text{-}ptr)_2(\mu_2\text{-}F)_2]_n(SiF_6)_n \cdot 2nH_2O$ (**4**), were synthesized with (*m*-phenol)-1,2,4-triazole (ptr). Compounds **1**–**4** with extended structures of 4-substituted 1,2,4-triazole are rarely reported. The layered structure of **1** can be regarded as constructed from the 2-D inorganic backbone of SO_4^{2-}(2) anions bridging $[Zn_4(\mu_3\text{-}OH)_2(H_2O)_2]^{6-}$ subunits with the ptr ligands anchoring to both sides of backbone. Compounds **2** and **3** are the first mercury(II) complexes with 4-substituted 1,2,4-triazole, which feature the ptr ligand acting as a bidentate ligand bridging the Hg(II) atoms to form arciform –Hg–ptr–Hg–ptr chains. The structure of **4** is constructed from the F atoms bridging Cu atoms in symmetrical μ_2-coordination mode to form a zigzag cationic chain with each ptr ligand bridging a pair of Cu atom on the both sides, resulting in a nonplanar 5-membered $[Cu_2N_2F]$ ring. Fluorescent properties of **1**–**4** were characterized and the magnetic property of **4** shows antiferromagnetic interaction between the copper(II) ions.

Keywords: Coordination polymers; (*m*-Phenol)-1,2,4-triazole; Crystal structure; Fluorescence; Magnetism

1. Introduction

The metal coordination polymers have been studied widely due to an important interface between synthetic chemistry and materials science, and specific structures, properties, and reactivities not found in mononuclear compounds. And synthesis of metal coordination polymers is attracting interest in understanding how molecules can be organized and how functions can be achieved [1–3]. Many attempts have been made to synthesize a variety of transitional metal complexes using the 1,2,4-triazole ligands, and their structures and properties have been physically and chemically determined. 1,2,4-triazoles have attracted great and growing interest in coordination chemistry because of the fact that they can synthesize transition metal coordination polymers with the two bridging close adjacent nitrogen atoms (N1 and N2) or the 4-positioned one (N4) [4], and can effectively transmit magnetic interaction between paramagnetic centers [5–9]. 1,2,4-triazoles also exhibiting excellent bioactivities have particularly multifarious uses in agriculture, medicine, and industry. 1,2,4-triazole as a readily available and inexpensive resource is also a good candidate to synthesize suitable nitrenium ion precursors [10] with their syntheses and synthetic applications [11–14] and implications as "ultimate carcinogens" from aromatic amines [15,16].

In view of the coordination character of 1,2,4-triazole, our interest is in the investigation of the triazole-bridging coordination polymers as well as their properties [17]. Herein, four coordination polymers were synthesized using (*m*-phenol)-1,2,4-triazole (ptr) ligand and the crystallographic structures and properties of fluorescence and magnetism were characterized.

*Corresponding author. Fax: +86 591 8371 4946.
E-mail address: gcguo@ms.fjirsm.ac.cn (G.-C. Guo).

0022-4596/$ - see front matter © 2006 Elsevier Inc. All rights reserved.
doi:10.1016/j.jssc.2006.05.046

2. Experimental

2.1. Materials and physical measurements

All reagents and solvents were used directly as supplied commercially without further purification. $CuSiF_6$ was prepared using verdigris and H_2SiF_6. The IR spectra were recorded on a Nicolet Magna 750 FT-IR spectrometer with KBr pellets in the range 4000–400 cm^{-1}. Elemental analyses were carried out on a Vario EL III elemental analyzer at the Analytical Center of this Institute. The electronic emission and excitation spectra recorded at room temperature were obtained by a Edinburgh FL/FS 920 TCSPC fluorescence spectrophotometer. Magnetic susceptibilities were measured with a quantum Design MPMS SQUID magnetometer in the temperature range 2–305 K with the applied magnetic field was 10,000 G.

2.2. Synthesis of (m-phenol)-1,2,4-triazole [18,19]

(*m*-Phenol)-1,2,4-triazole (ptr) was prepared by reacting the diformylhydrazine (6 mmol, 528 mg) and *m*-aminophenol (6 mmol, 654 mg) in a Teflon-lined stainless steel autoclave in a furnace at 443 K for 3 days and then cooled to 293 K (see Scheme 1). The product were isolated and washed with hot water and hot ethanol. The orange crystals suitable for X-ray diffraction studies were obtained. Yield based on *m*-aminophenol: 754 mg, 78%. Elemental analysis (%) for $C_8H_7N_3O$, found (calcd): C, 59.61 (59.62); H, 4.29 (4.38); N, 26.18 (25.90). IR (cm^{-1}, KBr): 3136(w), 3120(w), 2954(w), 2846(w), 2743(w), 1613(s), 1533(vs), 1494(s), 1388(w), 1381(m), 1293(s), 1204(s), 1093(m).

2.3. Synthesis of $[Zn_4(ptr)_2(SO_4)_3(\mu_3\text{-}OH)_2(H_2O)_4]_n$ (1)

The hydrothermal reaction of ptr (0.2 mmol, 32 mg) and $ZnSO_4 \cdot 5H_2O$ (0.2 mmol, 50 mg) with 10 mL mixed solvent of water and DMF (V/V = 1:1) at 443 K for 72 h resulted colorless prismatic crystals. Elemental analysis (%), found (calcd) for **1**: C, 19.68 (19.65); H, 2.45 (2.47); N, 8.61 (8.59). IR data (in KBr, cm^{-1}): 3398(s), 2974(m), 2925(m), 1629(m), 1449(w), 1412(w), 1381(m), 1274(w), 1089(s), 1050(s), 881(s), 803(m), 665(w).

2.4. Syntheses of $[Hg(CN)_2(ptr)]_n$ (2) and $[Hg(Cl)_2(ptr)]_n$ (3)

To 10 mL aqueous solution of ptr (0.2 mmol, 32 mg) was added 0.5 equiv. of mercury salt ($Hg(CN)_2$ for **2** and $HgCl_2$ for **3** at 353 K with stirring. The resulting solutions were filtered, and the red platelet crystals of **2** and **3** suitable for X-ray diffraction studies were obtained by slow evaporation of the filtrates at room temperature for a couple of weeks. Elemental analysis (%), found (calcd) for **2**: C, 29.11 (29.03); H, 1.75 (1.71); N, 16.89 (16.92); Found (calcd) for **3**: C, 22.17 (22.21); H, 1.66 (1.63); N, 9.74 (9.71). IR data (in KBr, cm^{-1}): for **2**: 3434(vs), 2974(m), 1602(s), 1530(m), 1453(m), 1384(m), 1290(w), 1205(w), 1091(m), 1050(m), 880(m), 780(w), 684(w), 645(w); for **3**: 3392(vs), 2975(vs), 1615(s), 1530(m), 1454(m), 1384(m), 1204(m), 1089(s), 1049(vs), 880(s), 687(w), 646(w).

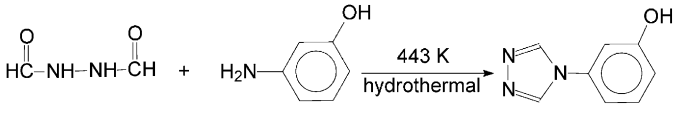

Scheme 1. The synthesis of (*m*-phenol)-1,2,4-triazole.

2.5. Synthesis of $[Cu_2(\mu_2\text{-}ptr)_2(\mu_2\text{-}F)_2]_n(SiF_6)_n \cdot 2nH_2O$ (4)

The hydrothermal reaction of 5 mL aqueous solution of ptr (0.2 mmol, 32 mg) and the aqueous solution of $CuSiF_6$ (0.2 mmol, 41 mg) at 393 K for 72 h resulted blue platelet crystals of **4**. Elemental analysis (%), found (calcd) for **4**: C, 28.90 (28.92); H, 2.76 (2.73); N, 12.68 (12.65). IR data (in KBr, cm^{-1}): 3435(s), 2924(m), 2851(m), 1619(m), 1544(w), 1498(w), 1460(w), 1392(w), 1299(w), 1218(w), 1108(w), 1068(w), 1013(w), 867(w), 784(w), 739(w), 683(w), 635(w).

2.6. X-ray crystallography

A summary of the crystallographic data for compounds **1–4** is given in Table 1. Data were collected on a Rigaku Mercury CCD diffractometer with graphite-monochromated Mo$K\alpha$ radiation ($\lambda = 0.71073$ Å) using an ω scan technique at 113 K. The intensity data were reduced using the CrystalClear program [20]. The structures were solved by direct methods using the SHELXTL package of crystallographic software [21] and refined by full-matrix least-squares technique on F^2. All nonhydrogen atoms were refined anisotropically and the hydrogen atoms were included in the final stage of the refinement on calculated positions bonded to their carrier atoms. Atoms O(1) in **2** and O(1) in **3** are positionally disordered. The selected bond distances and bond angles for **1–4** are listed in Tables 2–4.

Crystallographic data for the four structures reported here have been deposited with the Cambridge Crystallographic Data Centre (Deposition Nos. CCDC: 295285–295288 for **1–4**). The data can be obtained free of charge via www.ccdc.cam.ac.uk/conts/retrieving.html (or from the CCDC, 12 Union Road, Cambridge CB2 1EZ, UK; fax: +44 1223 336033; e-mail: deposit@ccdc.cam.ac.uk).

3. Results and discussion

3.1. Description of crystal structures

3.1.1. Structure of $[Zn_4(ptr)_2(SO_4)_3(\mu_3\text{-}OH)_2(H_2O)_4]_n$ (1)

X-ray single-crystal analysis shows there exist two kinds of independent zinc(II) atoms in the structure of **1**. The

Table 1
Crystallographic data and refinement parameters for **1**–**4**

	1	**2**	**3**	**4**
Empirical formula	$C_{16}H_{24}N_6O_{20}S_3Zn_4$	$C_{10}H_7HgN_5O$	$C_8H_7Cl_2HgN_3O$	$C_{16}H_{18}Cu_2F_8N_6O_4Si$
Color and habit	Colorless prism	Red platelet	Red platelet	Blue platelet
Crystal size (mm)	$0.1 \times 0.1 \times 0.1$	$0.58 \times 0.32 \times 0.11$	$0.48 \times 0.32 \times 0.11$	$0.1 \times 0.1 \times 0.04$
Crystal system	Monoclinic	Monoclinic	Monoclinic	Monoclinic
Space group	$C2/c$	$P2_1/c$	$P2_1/c$	$P2_1/c$
a (Å)	28.771(9)	6.6281(17)	6.4786(10)	13.273(6)
b (Å)	7.49465(19)	21.802(5)	22.614(2)	6.579(3)
c (Å)	15.132(48)	8.321(2)	7.9773(15)	13.931(6)
β (°)	117.148(4)	105.1050(10)	108.457(2)	115.1110(7)
V (Å^3)	2903.3(14)	1160.9(5)	1108.6(3)	1101.5(8)
Z	4	4	4	2
Fw	978.07	413.80	432.66	665.53
D_{calcd} (mg m^{-3})	2.238	2.368	2.592	2.007
μ (mm^{-1})	3.583	13.248	14.340	2.093
$F(0\,0\,0)$	1960	760	792	664
θ (°)	3.03–5.02	3.15–5.02	3.32–5.03	3.39–5.02
Reflections measured	8901	7186	6492	6739
Independent reflections	2553 ($R_{int} = 0.0593$)	2023 ($R_{int} = 0.0479$)	1894 ($R_{int} = 0.0357$)	1943 ($R_{int} = 0.0761$)
Observed reflection	2013	1553	1589	1493
Final R_1, wR_2 [$I > 2\sigma(I)$]	0.0439, 0.0873	0.0421,0.0950	0.0344,0.0872	0.0620, 0.1179
R indices (all)	0.0632, 0.0948	0.0488,0.0965	0.0413, 0.0907	0.0900, 0.1321
GOF on F^2	1.067	1.007	1.023	1.082
$(\Delta/\sigma)_{max/min}$	0.000, 0.000	0.001,0.000	0.002,0.000	0.000, 0.000
Largest difference peak/eÅ^{-3}	0.745, −0.441	1.388, −3.492	1.822, −1.360	0.686, −0.483

Table 2
Selected bond distances (Å) and angles (deg.) for $[Zn_4(ptr)_2(SO_4)_3(\mu_3\text{-}OH)_2(H_2O)_4]_n$ (**1**)

Zn1–O7	2.053(3)	Zn2–O1W	2.066(3)
Zn1–N12A	2.072(4)	Zn2–O7A	2.077(3)
Zn1–O2W	2.113(3)	Zn2–O3	2.100(3)
Zn1–O2	2.115(3)	Zn2–O7	2.105(3)
Zn1–O4B	2.124(3)	Zn2–N11	2.141(4)
Zn1–O5	2.287(3)	Zn2–O5	2.336(3)
O7–Zn1–N12A	92.41(14)	O1W–Zn2–N11	90.41(14)
O7–Zn1–O2W	176.36(12)	O7A–Zn2–N11	89.19(13)
N12A–Zn1–O2W	87.86(14)	O3–Zn2–N11	86.73(13)
O7–Zn1–O2	93.65(12)	O7–Zn2–N11	110.20(13)
N12A–Zn1–O2	169.19(14)	O1W–Zn2–O5	81.50(12)
O2W–Zn1–O2	86.65(12)	O7A–Zn2–O5	98.91(11)
O7–Zn1–O4B	98.76(12)	O3–Zn2–O5	86.20(12)
N12A–Zn1–O4B	96.92(13)	O7–Zn2–O5	78.00(11)
O2W–Zn1–O4B	77.61(12)	N11–Zn2–O5	169.42(12)
O2–Zn1–O4B	91.00(11)	C12–N11–Zn2	132.1(3)
O7–Zn1–O5	80.20(11)	N12–N11–Zn2	121.7(3)
N12A–Zn1–O5	85.69(12)	C11–N12–Zn1A	132.6(3)
O2W–Zn1–O5	103.44(12)	N11–N12–Zn1A	119.4(3)
O2–Zn1–O5	86.53(11)	S1–O2–Zn1	122.84(18)
O4B–Zn1–O5	177.24(11)	S1–O3–Zn2	124.53(17)
O1W–Zn2–O7A	100.19(12)	S1–O4–Zn1B	133.46(19)
O1W–Zn2–O3	88.19(12)	S2–O5–Zn1	131.03(18)
O7A–Zn2–O3	170.71(12)	S2–O5–Zn2	128.72(18)
O1W–Zn2–O7	159.38(13)	Zn1–O5–Zn2	90.88(11)
O7A–Zn2–O7	80.99(12)	Zn1–O7–Zn2A	117.05(14)
O3–Zn2–O7	92.60(11)	Zn1–O7–Zn2	104.76(13)
		Zn2A–O7–Zn2	99.01(12)

Note: Symmetry code: A = $-x$, $-y+4$, $-z+1$; B = $-x$, $-y+3$, $-z+1$.

Table 3
Selected bond distances (Å) and angles (deg.) for $[Hg(CN)_2(trp)]_\infty$ (**2**) and $[Hg(Cl)_2(trp)]_\infty$ (**3**)

2		**3**	
Hg1–C1	2.067(3)	Hg1–N12A	2.350(2)
Hg1–C2	2.068(4)	Hg1–Cl1	2.3595(9)
Hg1–N12A	2.576(3)	Hg1–Cl2	2.3677(7)
Hg1–N11	2.586(4)	Hg1–N11	2.583(3)
N11–C18	1.299(5)	N11–C18	1.306(4)
N11–N12	1.396(4)	N11–N12	1.360(3)
N12–C17	1.267(5)	N12–C17	1.309(4)
N13–C17	1.346(4)	C11–N13	1.442(4)
N13–C18	1.350(5)	C17–N13	1.353(3)
C1–Hg1–C2	164.30(16)	N12A–Hg1–Cl1	111.05(6)
C1–Hg1–N12A	97.80(12)	N12A–Hg1–Cl2	100.53(6)
C2–Hg1–N12A	95.79(13)	Cl1–Hg1–Cl2	147.56(3)
C1–Hg1–N11	96.99(12)	N12A–Hg1–N11	90.16(9)
C2–Hg1–N11	91.57(14)	Cl1–Hg1–N11	93.10(6)
N12A–Hg1–N11	86.75(11)	Cl2–Hg1–N11	94.05(5)
C18–N11–Hg1	122.8(3)	C18–N11–Hg1	125.8(2)
N12–N11–Hg1	127.6(2)	N12–N11–Hg1	123.41(18)
C17–N12–Hg1B	128.7(3)	C17–N12–Hg1B	125.1(2)
N11–N12–Hg1B	123.3(2)	N11–N12–Hg1B	127.7(2)
N1–C1–Hg1	178.1(4)		
N2–C2–Hg1	175.8(4)		

Note: Symmetry code: A = x, $-y+0.5$, $z+0.5$; B = x, $-y+0.5$, $z-0.5$.

zinc(II) atoms have six-coordinate octahedral geometries (4+2) (Fig. 1). The Zn1 atom in its coordination environment is coordinated by O2 from SO_4^{2-}, N12A (A = $-x$, $4-y$, $1-z$) from ptr occupying the axial positions, and O4B (B = $-x$, $3-y$, $1-z$), O5 from SO_4^{2-}, O2W, and μ_3-O7 lying on the equatorial plane; the octahedral geometry of the Zn2 atom is formed by O5, μ_3-O7, O1W, and N11 in its equatorial plane, and μ_3-O7A, O3 in its axial positions. The oxidation state of O7 is −1, estimated by the bond–valence–sum (BVS) calculation being 1.093, showing that O7 should be OH^- anions, in accord with the judge from the charge balance. The OH^- ion adopts an asymmetric μ_3-coordinate mode to bridge three Zn(II) atoms, with the Zn2–O7 bond distances (2.105(3) Å) being longer than the other ones (Zn1–O7 = 2.053(3); Zn2–O7 = 2.077(3) Å). Two μ_3-O7 ions bridge three zinc(II) atoms to form a negative subunit of $[Zn_4(\mu_3\text{-}OH)_2(H_2O)_2]^{6-}$. The subunits are double-bridged by SO_4^{2-}(1) groups to form 1-D zigzag chains extending along the *b* direction, which are further bridged by SO_4^{2-}(2) groups to form a 2-D inorganic backbone along the *c* direction as shown in Fig. 2. The ptr ligand acts as a terminal ligand to bridge two Zn atoms of the subunit on the both sides of the backbone (Fig. S1). Therefore, the layered structure of **1** can be regarded as constructed from the 2-D inorganic backbone of SO_4^{2-}(2) anions bridging $[Zn_4(\mu_3\text{-}OH)_2(H_2O)_2]^{6-}$ subunits with the ptr ligands anchoring to the both sides of backbone.

There are abundant hydrogen bondings in the layer: O1W···O1A (2.688(5) Å, A = x, $1+y$, z), O1W···O6B (2.690(5) Å, B = $-x$, y, $0.5-z$), O2W···O2B (2.694(5) Å), O2W···O6C (2.892(5) Å, $C = x$, $y-1$, z). And the layers are further connected by hydrongen bonding O11···O1D (2.823(5) Å, 172.7°, D = $-0.5-x$, $3.5-y$, $1-z$) along the *b*-axis to form 3-D framework (Fig. S2). Though phenyl rings are present, there are no $\pi\cdots\pi$ stacking interactions in the 3-D structure, with the minimum centroid-to-centroid distances being 3.856 Å.

Table 4
Selected bond distances (Å) and angles (deg.) for $[Cu_2(\mu_2\text{-ptr})_2(\mu_2\text{-}F)_2]_n(SiF_6)_n \cdot 2nH_2O$ (**4**)

Cu1–F1	1.9245(16)
Cu1–F1A	1.9296(16)
Cu1–N12	1.987(2)
Cu1–N11A	2.014(2)
F1–Cu1–F1A	176.72(3)
F1–Cu1–N12	88.46(7)
F1A–Cu1–N12	89.09(7)
F1–Cu1–N11A	93.48(7)
F1A–Cu1–N11A	88.99(8)
N12–Cu1–N11A	178.05(7)
C15–N11–Cu1B	136.75(17)
N12–N11–Cu1B	116.30(14)
C13–N12–Cu1	131.99(17)
N11–N12–Cu1	121.13(14)
Cu1–F1–Cu1B	117.28(7)

Note: Symmetry code: $A = -x, y+0.5, -z+0.5$; $B = -x, y-0.5, -z+0.5$.

3.1.2. *Structures of $[Hg(CN)_2(ptr)]_n$ (**2**) and $[Hg(Cl)_2(ptr)]_n$ (**3**)*

Compounds **2** and **3** are the first extending mercury(II) complexes with 1,2,4-triazole and the first mercury(II) complexes with 4-substituted 1,2,4-triazole, the other examples of 1,2,4-triazole only being three [22–24]. The molecular structures of **2** and **3** are isomorphous with similar cell parameters except that the anion CN^- in **2** and Cl^- in **3**, so the two complexes will be discussed together.

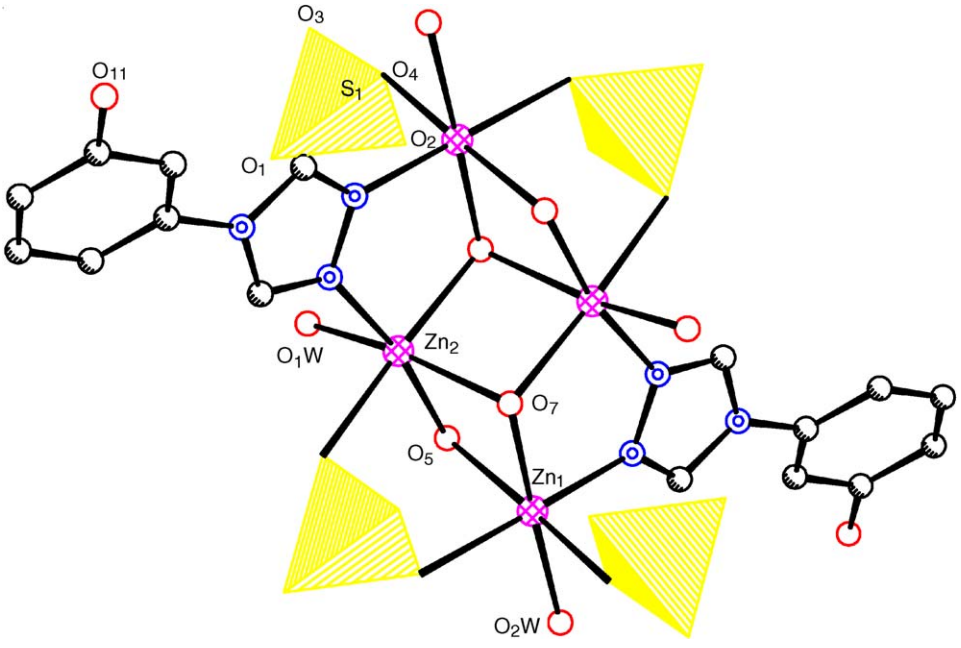

Fig. 1. The coordination environments of Zinc(II) atoms in **1** with 40% thermal ellipsoids.

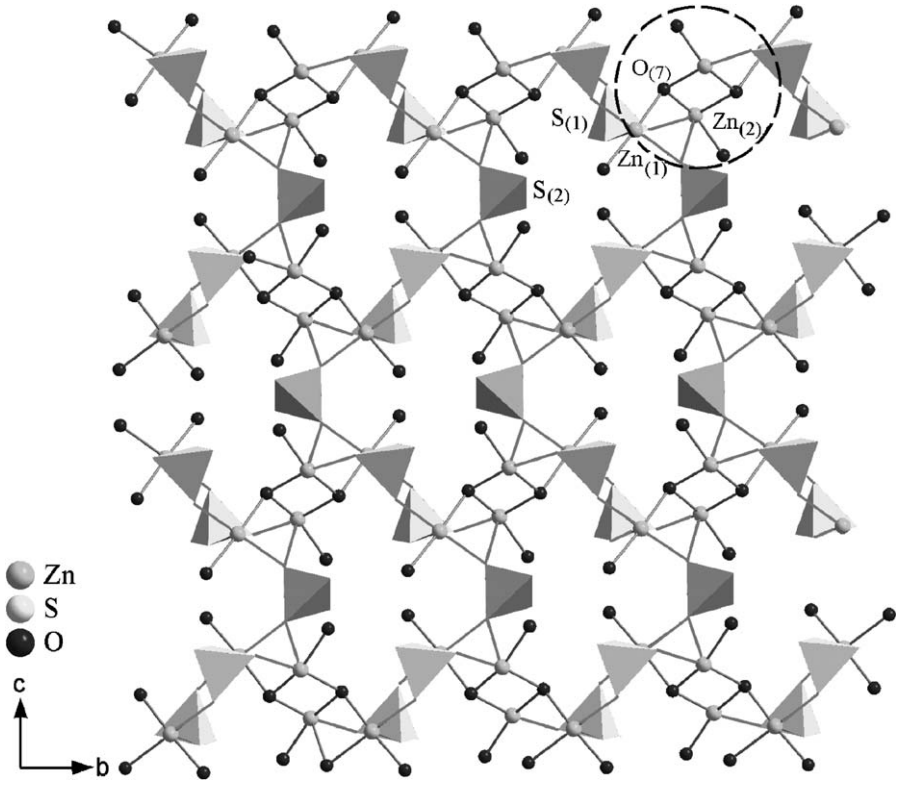

Fig. 2. The 2-D layer in **1** constructed from the $[Zn_4(\mu_3\text{-}OH)_2(H_2O)_2]^{6-}$ subunits (the part in dash circle) connecting with two kinds of SO_4^{2-} [polyhedra S(1) and S(2) denoted as SO_4^{2-}(1) and SO_4^{2-}(2) respectively; the ptr ligands are omitted for clarity.

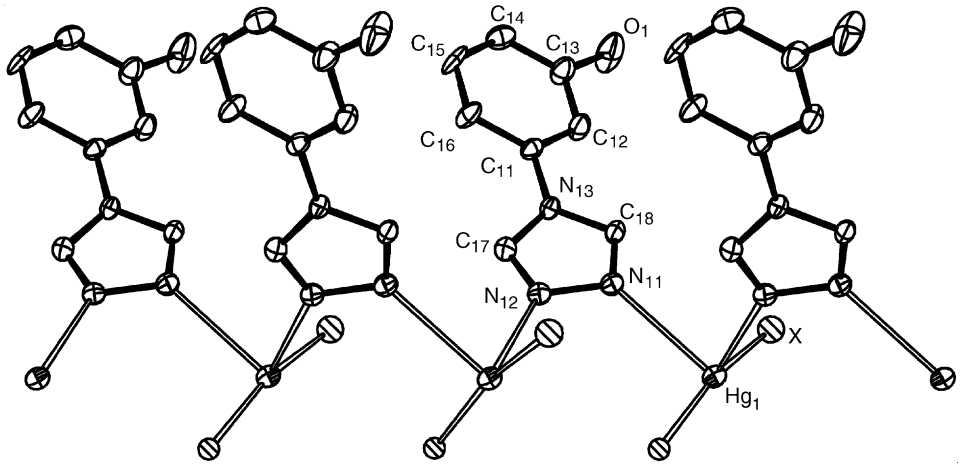

Fig. 3. The arciform chain extending along the *c*-axis (X = CN for **2**, Cl for **3**).

X-ray single crystal analyses reveal that the crystallographic asymmetric units in **2** and **3** both comprise one mercury(II) salt and one ptr molecule as shown in Fig. S3. The ptr ligand acts as a bidentate ligand bridging the Hg(II) atoms via the nitrogen atoms N11 and N12, resulting in an arciform –Hg–ptr–Hg–ptr chain running along the *c*-axis (Fig. 3). The center atom Hg(II) lies in a distorted tetrahedron geometry, consisting of two nitrogen atoms from two different ptr moieties and two X anions (X = CN for **2**, Cl for **3**). However, the Hg–N bond distances in **2** and **3** are not similar: The Hg1–N11 bond distance of 2.583(3) Å in **3** is much longer than the other Hg1–N12A bond distance of 2.350(2) Å; the two Hg–N bond distances in **2** are almost equal (Hg1–N11 = 2.586(4) Å; Hg1–N12A = 2.576(3) Å, A = x, $-y+0.5$, $z+0.5$). The range of C=N double bond distances in **2** and **3** is between 1.267(5) and 1.309(4) Å, similar to those found in the ligand ptr between 1.299(3) and 1.302(4) Å.

The neighboring arciform chains of **2** and **3** interconnect to form 18-membered rings through hydrogen bonds (In **2**, O1–H···N2: 2.855 Å, 169.24°; in **3**, O1–H···Cl1: 3.100 Å, 168.698°) and result in a 2-D wavy layer along the *bc* plane (Fig. S4). The minimum centroid-to-centroid distance of 6.03 Å among phenyl rings or triazole rings shows no $\pi\cdots\pi$ stacking interactions in the crystal structures. The layers stack parallel along the *a* direction to form the crystal structure (Fig. S5).

3.1.3. Structure of $[Cu_2(\mu_2\text{-ptr})_2(\mu_2\text{-}F)_2]_n(SiF_6)_n\cdot 2nH_2O$ (**4**)

The asymmetrical unit of **4** contains a positive subunit of $[Cu(\mu_2\text{-}F)(\mu_2\text{-ptr})]^+$, half of a dissociative SiF_6^{2-} ion, and a water lattice. The Cu1 atom is coordinated by F1, F1A, N12, and N11A ($A = -x,\ 0.5+y,\ 0.5-z$) atoms with Cu1–F1 = 1.9245(16), Cu1–F1A = 1.9296(16), Cu1–N12 = 1.987(2), and Cu1–N11A = 2.014(2) Å ($A = -x,\ y+0.5,\ -z+0.5$) to form a planar quadrangle. F^- ions originated from the thermal decomposability of SiF_6^{2-} as the source of F^- ions were not included in the reactants [25]. The structure of **4** can be regarded as constructed from the F atoms bridging Cu atoms in symmetrical μ_2-coordination mode extending along the *b* direction to form a zigzag cationic chain with each ptr ligand bridging a pair of Cu atom on the both sides, resulting in a nonplanar 5-membered $[Cu_2N_2F]$ ring (Fig. 4). The minimum centroid-to-centroid distance of phenyl rings is 4.553 Å, indicating no $\pi\cdots\pi$ stacking interactions in the crystal structures. The lattice water molecules double-bridge the SiF_6^{2-} anions via O···F hydrogen bondings (O1W···F11 = 2.775(7), O1W···F12 = 2.896(6) Å) along the *b* direction to form anionic chains, which further link the cationic chains via O···O hydrogen bonds (O1–H···O1W = 2.692(3) Å, 179.2°) along the *a* direction to form a layered structure (Fig. S6). The layers stack in –ABAB– fashion along the *c* direction to yield the crystal structure (Fig. S7).

For the triazoles with three N positions unsubstituted, there are four kinds of coordination modes: monodentate, μ_2-N1,N2, μ_2-N2,N4, and μ_3-N1,N2,N4 (anionic ring). The μ_2-N1,N2 bridging mode for triazole preferably results in the formation of linear trinuclear metal complexes $[M_3(trz)_{6+x}(L)_{6-x}]$ [26–30] (trz = 1,2,4-triazoles; L = H_2O, SCN^-, N_3^-, etc.), while the bridging modes of μ_2-N2,N4 or μ_3-N1,N2,N4 for the triazoles usually results in the formation of extended structures. Generally, it is more difficult to synthesize mononuclear metal–triazole complexes, especially for first-row transition metals. There exist only 20 examples about mononuclear metal–triazole complexes [31–44]. In comparison with unsubstituted triazole, the 4-substituted triazoles lose a coordination site and can only act as mono- or μ_2-N1,N2 bridging bidentate ligands, which makes it difficult to construct extended structure. To our knowledge, the extended structures of 4-substituted 1,2,4-triazole-bridging transition metal complexes are rare, the known examples only being $[Cu(hyetrz)_3](CF_3SO_3)_2\cdot H_2O$ (hyetrz = 4-(2′-hydroxyethyl)-1,2,4-triazole) [45], $\{[Cd_3(deatrz)_2Cl_6(H_2O)_2]\cdot 2H_2O\}_n$, $\{[Cd_3(deatrz)_4Cl_2(SCN)_4]\cdot 2H_2O\}_n$ (deatrz = 3,5-diethyl-4-amino-1,2,4-triazole) [46], $\{[Cu(\mu_2\text{-amtrz})_3](BF_4)(SiF_6)_{0.5}\cdot 2H_2O\}_n$, $\{[Cu(\mu_2\text{-amtrz})_3](SiF_6)\cdot 8/3H_2O\}_n$ ((amtrz = 4-amino-1,2,4-triazole) [47], $\{[Cu_3(\mu_2\text{-L})_9](ClO_4)_6\cdot 9H_2O\}_n$ (L = 4-(2-hydroxyethyl)-1,2,4-triazole) [48], $[Fe(btr)_3]$

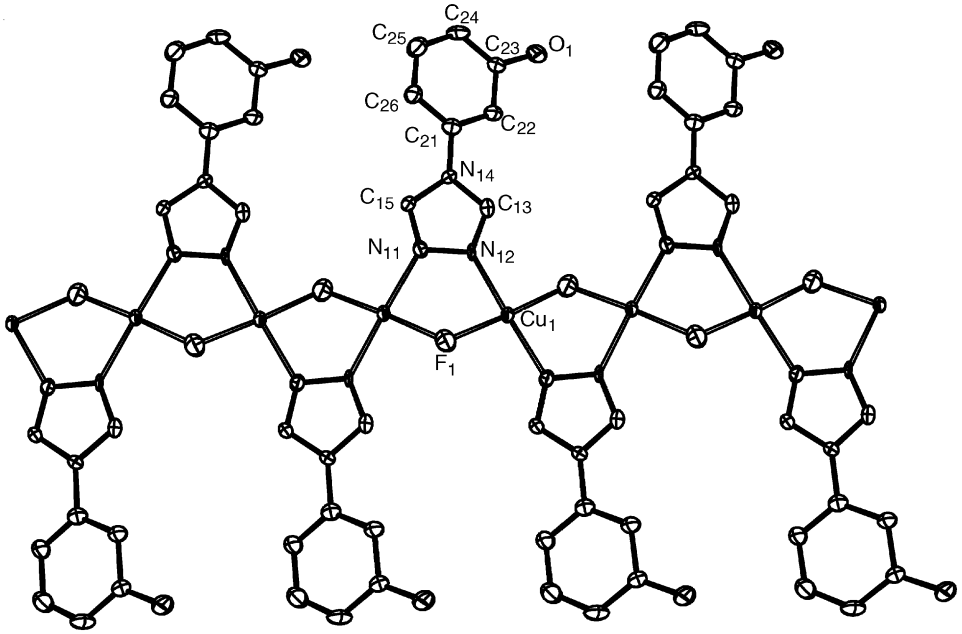

Fig. 4. The wavy chain extending along the *b*-axis in **4**.

$(ClO_4)_2$ (btr = 4,4-bis-1,2,4-triazole) [49] and $Fe(btr)_2(SeCN)_2 \cdot H_2O$ [50].

3.2. Fluorescent properties of 1–4

The fluorescent studies of 1,2,4-triazoles are very limited in contrast to the studies of magnetic properties. The compounds **1–4** reported here show luminescent features in the solid-state electronic emission spectra at room temperature, as given in Fig. 5. Green fluorescence for **1** can be observed, where the maximum emission wavelength is at 520 nm by exciting the solid sample under UV at $\lambda_{ex} = 298$ nm. Excitation of the solid sample **2** with UV ray at 361 nm produces blue fluorescence with intensive dual broad luminescence: a high-energy band around 445 nm and a lower energy emission around 415 nm appearing as a shoulder. The emission spectrum of **3** is similar to that of **2**: blue fluorescence with 440 and 420 nm as shoulder under UV at $\lambda_{ex} = 363$ nm. Compound **4** features blue fluorescence with a broad emission at 460 nm excited at 360 nm. Compared to the pure ligand of ptr (the emission at 450 nm with $\lambda_{ex} = 370$ nm) [51], the emissions near 450 nm for **1–4** may originate from the π–π^* transition of the triazole rings, not the phenyl rings (the emission of *m*-aminophenol at 405 nm with $\lambda_{ex} = 307$ nm, Fig. S8). The other emissions at 415 nm for **2** and 420 nm for **3** may be original from ligand-to-metal transfer (LMCT) [52,53]. Interestingly, the emission spectrum of **1** is much different from those of **2–4**; its excitation wavelength is much lower than 360 nm and its emission wavelength much higher than 450 nm, possibly relating to the 2-D inorganic backbone rather than the organic ligand.

3.3. The magnetic property of 4

The magnetic behavior of **4** is shown in Fig. 6 in the form of a χ_m vs. T and $\chi_m T$ vs. T plots. The produce $\chi_m T$ increases with the temperature rising, reaching a maximum of $0.725\,cm^3\,K\,mol^{-1}$ at ca. 258 K. Compound **4** follows the Curie–Weiss law $\chi_m = 0.40/(T + 0.30)$ in the temperature range 50–300 K. The magnetic behavior of **4** is characterized as an overall antiferromagnetic interaction between the copper(II) ions. An effective magnetic moment of $1.78\,\mu_B$ can thus be obtained for each Cu(II) center via $\mu_{eff} = 2.828C^{1/2}\,\mu_B$, which is very close to the theoretic $1.73\,\mu_B$ for the free-ion ground state ($^2D_{2/5}$) of Cu(II) with one localized unpaired *d*-electron. The magnetic data have been interpreted using the expression for the molar magnetic susceptibility of an $S = 1/2$ linear chain with a high-temperature series expansion proposed by Baker (Eq. (1)) [54] in which $x = J/2kt$, N is Avogadro's number, β is Bohr's magneton, k is Boltzmann's constant, and J is the isotropic exchange parameter defined by the phenomenological spin Hamiltonian $H = -J[\Sigma_{i<j}S_i \cdot S_j] - g\mu_B H \Sigma_i S_i$. The best least-squares fit of the theoretical equation to experimental data leads to $g = 2.080(8)$, $J/k = -2.76(1)$K, and the agreement factor $R = 3.75 \times 10^{-5}$ [$R = \{[\Sigma_{i=1}^{n}(\chi_{mi}^{exp} - \chi_{mi}^{calc})^2/(\chi_m)^{exp} i^2]/[\Sigma_{i=1}^{n}/(\chi_{mi}^{exp})^2]\}^{1/2}$]. The negative J value suggests that a weak antiferromagnetic interaction exists in **4**, which is in agreement with the result of the fitting obtained from the Curie–Weiss law. The antiferromagnetic property of 4 is similar to that of the 1-D chain of triazole $[Cu_2Cl_4(Mebta)_2]_n$ (Mebta = 1-methylbenzotriazole) [55], but unlike the ferromagnetic interaction in the 1-D chain of triazoles [Cu(hyetrz)$_3$]

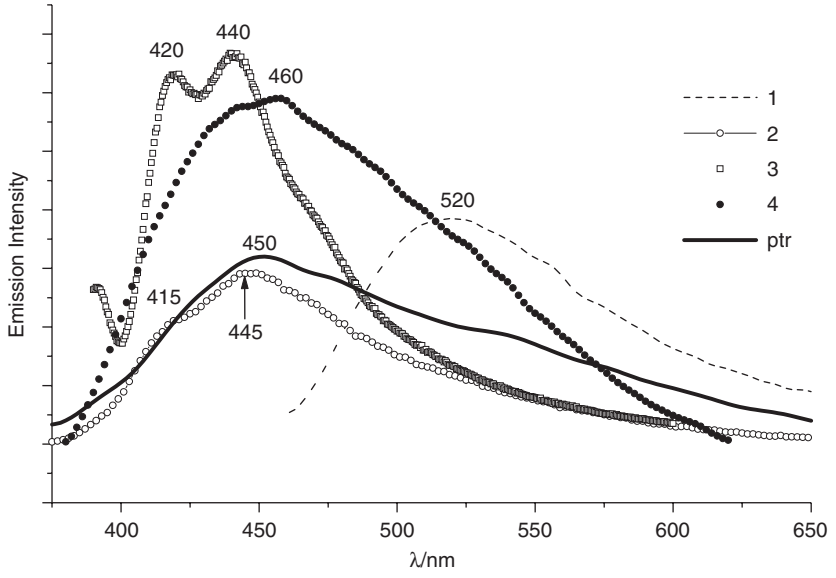

Fig. 5. The solid-state electronic emission spectra of **1** ($\lambda_{ex} = 298$ nm), **2** ($\lambda_{ex} = 361$ nm) **3** ($\lambda_{ex} = 363$ nm), **4** ($\lambda_{ex} = 360$ nm) and ptr ($\lambda_{ex} = 370$ nm) recorded at room temperature.

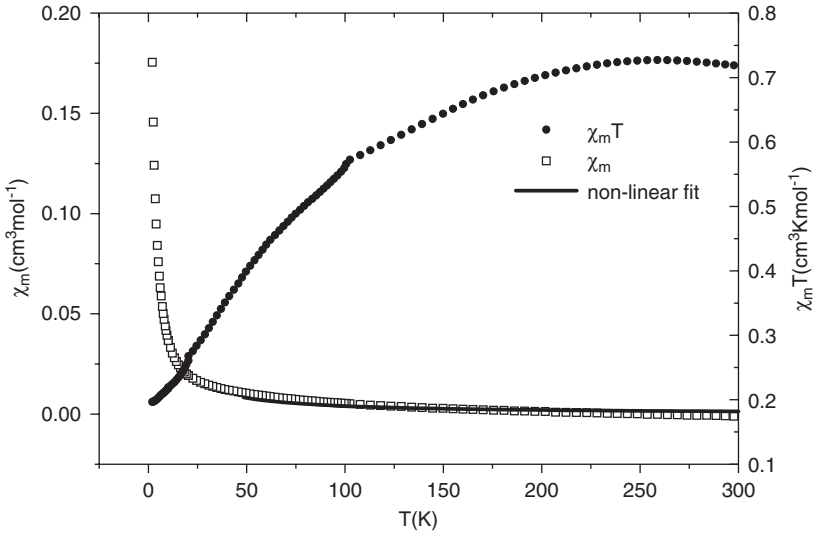

Fig. 6. Plot of χ_m vs. T over 2–300 K at a field of 1 T showing a Curie–Weiss paramagnetic behavior of **4**.

$(CF_3SO_3)_2 \cdot H_2O$ [12]:

$$\chi_m = \left(\frac{N\beta^2 g^2}{4kT}\right)\left(\frac{1 + 5.7979916x + 16.902653x^2 + 29.376885x^3 + 29.832959x^4 + 14.036918x^5}{1 + 2.7979916x + 7.0086780x^2 + 8.6538644x^3 + 4.5743114x^4}\right)^{2/3}. \quad (1)$$

The X-band powder EPR spectrum recorded at room temperature shows a signal with $g = 1.95$, which is consistent with the value from the fitting of the magnetic susceptibility data. Furthermore, Cu···Cu exchange splittings are not observed in the characterization [56].

Acknowledgments

We gratefully acknowledge the financial support of the NSF of China (20571075), the NSF for Distinguished Young Scientists of China (20425104), and the NSF of Fujian Province (A0420002).

Appendix A. Supplementary materials

Supplementary data associated with this article can be found in the online version at doi:10.1016/j.jssc.2006.05.046

References

[1] B. Zhao, P. Cheng, Y. Dai, C. Cheng, D.Z. Liao, S.P. Yan, Z.H. Jiang, G.L. Wang, Angew. Chem. Int. Ed. 42 (2003) 934.
[2] D.L. Reger, R.F. Semeniuc, M.D. Smith, J. Chem. Soc. Dalton Trans. (2003) 285.
[3] L. Shen, Y.Z. Xu, J. Chem. Soc. Dalton Trans. (2001) 3413.
[4] J.H. van Diemen, J.G. Haasnoot, R. Hage, J. Reedijk, J.G. Vos, R.J. Wang, Inorg. Chem. 30 (1991) 4038.
[5] P.M. Slangen, P.J. van Koningsbruggen, K. Goubitz, J.G. Haasnoot, J. Reedijk, Inorg. Chem. 33 (1994) 1121.
[6] P.J. van Koningsbruggen, J.G. Haasnoot, H. Kooijman, J. Reedijk, A.L. Spek, Inorg. Chem. 36 (1997) 2487.
[7] Y. Garcia, P.J. van Koningsbruggen, G. Bravic, P. Guionneau, D. Chasseau, G.L. Cascarano, J. Moscovici, K. Lambert, A. Michalowicz, O. Kahn, Inorg. Chem. 36 (1997) 6357.
[8] P.J. van Koningsbruggen, J.W. van Hal, R.A.G. de GraaV, J.G. Haasnoot, J. Reedijk, J. Chem. Soc. Dalton Trans. (1993) 2163.
[9] J.C. Liu, D.G. Fu, J.Z. Zhuang, C.Y. Duan, X.Z. You, J. Chem. Soc. Dalton Trans. (1999) 2337.
[10] R.A. Abramovitch, H.H. Gibson, S. Olivella, J. Org. Chem. 66 (2001) 1242.
[11] R.A. Abramovitch, P. Chinnasamy, K. Evertz, G. Huttner, J. Chem. Soc. Chem. Commun. (1989) 3.
[12] J.D.F. DeSousa, J.A.R. Rodrigues, R.A. Abramovitch, J. Am. Chem. Soc. 116 (1994) 9745.
[13] R.A. Abramovitch, X.-C. Ye, W.T. Pennington, G. Schimek, D. Bogdal, J. Org. Chem. 65 (2000) 343.
[14] H. Takeuchi, J. Chem. Soc. Chem. Commun. (1987) 961.
[15] M. Novak, L.L. Xu, R.A. Wolf, J. Am. Chem. Soc. 120 (1998) 1643.
[16] W.G. Humphreys, F.F. Kadlubar, F.P. Guengerich, Proc. Natl. Acad. Sci. USA 89 (1992) 8278.
[17] J.-C. Liu, G.-C. Guo, J.-S. Huang, X.-Z. You, Inorg. Chem. 42 (2003) 235.
[18] R.H. Wiley, A.J. Hart, J. Org. Chem. 18 (1953) 1368.
[19] C. Foces-Foces, P. Cabildo, R.M. Claramunt, J. Elguero, Acta Crystallogr. Sect. C Cryst. Struct. Commun. 55 (1999) 1160.
[20] Rigaku, CrystalClear 1.35, Software User's Guide for the Rigaku, *R*-Axis, Mercury and Jupiter CCD Automated X-ray Imaging System, Rigaku Molecular Structure Corporation, 2002.
[21] Siemens, SHELXTL Version 5 Reference Manual, Siemens Energy and Automation Inc., Madison, Wisconsin, USA, 1994.
[22] J.M. Salas, J.A.R. Navarro, M.A. Romero, M. Quirós, An. Quim. Int. Ed. 93 (1997) 55.
[23] J. Dillen, A.T.H. Lenstra, J.G. Haasnoot, J. Reedijk, Polyhedron 2 (1983) 195.

[24] J.M. Salas, M.A. Romero, A. Rahmani, R. Faure, G.A.D. Cienfuegos, E.R.T. Tiekink, J. Inorg. Biochem. 64 (1996) 259.
[25] P.J. van Konigsbruggen, J.G. Hassnoot, R.A.G. de Graaff, J. Reedijk, J. Chem. Soc. Dalton Trans. (1993) 483.
[26] L. Antolini, A.C. Fabretti, D. Gatteschi, A. Giusti, R. Sessoli, Inorg. Chem. 30 (1991) 4858.
[27] J.J.A. Kolnaar, G. van Dijk, H. Kooijman, A.L. Spek, V.G. Ksenofontov, P. Gutlich, J.G. Haasnoot, J. Reedijk, Inorg. Chem. 36 (1997) 2433.
[28] Y. Garcia, P. Guionneau, G. Bravic, D. Chasseau, J.A.K. Howard, O. Khan, V. Ksenofontov, S. Reiman, P. Gutlich, Eur. J. Inorg. Chem. (2000) 1531.
[29] J.C. Liu, Y. Song, Z. Yu, J.Z. Zhuang, X.Y. Huang, X.Z. You, Polyhedron 18 (1999) 1491.
[30] W. Vreugdenhil, J.G. Haasnoot, J. Reedijk, J.S. Wood, Inorg. Chim. Acta 167 (1990) 109.
[31] C. Yelamos, K.R. Gust, G.A. Baboul, M.J. Heeg, H.B. Schlegel, C.H. Winter, Inorg. Chem. 40 (2001) 6451.
[32] P. Passaniti, W.R. Browne, F.C. Lynch, D. Hughes, M. Nieuwenhuyzen, P. James, M. Maestri, J.G. Vos, J. Chem. Soc. Dalton Trans. (2002) 1740.
[33] N.C. Mosch-Zanetti, M. Hewitt, T.R. Schneider, J. Magull, Eur. J. Inorg. Chem. 1 (2002) 1181.
[34] C. Sanchez, J.M. Salas, M. Quiros, M.P. Sanchez, Acta Crystallogr. Sect. E Struct. Rep. Online 60 (2004) m370.
[35] W.R. Browne, C.M. O'Connor, H.P. Hughes, R. Hage, O. Walter, M. Doering, J.F. Gallagher, J.G. Vos, J. Chem. Soc. Dalton Trans. (2002) 4048.
[36] N.V. Podberezskaya, N.V. Pervukhina, V.P. Doronina, Zh. Strukt. Khim. Russ. 32 (1991) 33–34.
[37] A.C. Fabretti, J. Crystallogr. Spectrosc. Res. 22 (1992) 523.
[38] L.F. Tang, Z.H. Wang, J.F. Chai, X.B. Leng, J.T. Wang, H.G. Wang, J. Organomet. Chem. 642 (2002) 179.
[39] C. Faulmann, P.J. van Koningsbruggen, R.A. G.de Graaf, J.G. Haasnoot, J. Reedijk, Acta Crystallogr. Sect. C Cryst. Struct. Commun. 46 (1990) 2357.
[40] R. Hage, J.G. Haasnoot, J. Reedijk, R. Wang, E.M. Ryan, J.G. Vos, A.L. Spek, A.J.M. Duisenberg, Inorg. Chim. Act 174 (1990) 77.
[41] W.R. Browne, D. Hesek, J.F. Gallagher, C.M. O'Connor, J.S. Killeen, F. Aoki, H. Ishida, Y. Inoue, C. Villani, J.G. Vos, Dalton Trans. (2003) 2597.
[42] B.E. Buchanan, J.G. Vos, M. Kaneko, W.J.M. van der Putten, J.M. Kelly, R. Hage, R.A.G. de Graaff, R. Prins, J.G. Haasnoot, J. Reedijk, J. Chem. Soc. Dalton Trans. 1 (1990) 2425.
[43] B. Mehmetaj, J.G. Haasnoot, L. De Cola, G.A. van Albada, I. Mutikainen, U. Turpeinen, J. Reedijk, Eur. J. Inorg. Chem. (2002) 1765.
[44] F. Gaccioli, R. Franchi-Gazzola, M. Lanfranchi, L. Marchio, G. Metta, M.A. Pellinghelli, S. Tardito, M. Tegoni, J. Inorg. Biochem. 99 (2005) 1573.
[45] Y. Garcia, P.J. van Koningsbruggen, G. Bravic, D. Chasseau, O. Kahn, Eur. J. Inorg. Chem. (2003) 356.
[46] L. Yi, B. Ding, B. Zhao, P. Cheng, D.-Z. Liao, S.-P. Yan, Z.-H. Jiang, Inorg. Chem. 43 (2004) 33.
[47] K. Drabent, Z. Ciunik, Chem. Commun. (2001) 1254.
[48] Y. Garcia, P.J. van Koningsbruggen, G. Bravic, P. Guionneau, D. Chasseau, G.L. Cascarano, J. Moscovici, K. Lambert, A. Michalowicz, O. Kahn, Inorg. Chem. 36 (1997) 6357.
[49] Y. Garcia, O. Kahn, L. Rabardel, B. Chansou, L. Salmon, J.P. Tuchagues, Inorg. Chem. 38 (1999) 4663.
[50] A. Ozarowski, S.Z. Yu, B.R. McGarvey, A. Mislanker, J.E. Drake, Inorg. Chem. 30 (1991) 3167.
[51] L. Xu, G.-C. Guo, B. Liu, M.-L. Fu, J.-S. Huang, Acta Crystallogr. E60 (2004) O1060.
[52] H. Han, Y.L. Song, H.W. Hou, Y.T. Fan, Y. Zhu, J. Chem. Soc. Dalton Trans. (2006) 1972.
[53] B. Ding, L. Yi, Y. Wang, P. Cheng, D.Z. Liao, S.P. Yan, Z.H. Jiang, H.B. Song, H.G. Wang, J. Chem. Soc. Dalton Trans. (2006) 665.
[54] G.A. Baker, G.S. Rushbrooke, H.E. Gilbert, Phys. Rev. A 135 (1964) 1272.
[55] K. Skorda, T.C. Stamatatos, A.P. Vafiadis, A.T. Lithoxoidou, A. Terzis, S.P. Perlepes, J. Mrozinski, C.P. Raptopoulou, J.C. Plakatouras, E.G. Bakalbassis, Inorg. Chim. Acta 358 (2005) 565.
[56] B.J. Hathaway, D.E. Billing, Coord. Chem. Rev. 5 (1972) 143.